Front. Biol. 2013, 8(5): 549–555
DOI 10.1007/s11515-013-1277-8

RESEARCH ARTICLE

Oxidative-damage effect of Fe_3O_4 nanoparticles on mouse hepatic and brain cells *in vivo*

Yongli WANG *, Nian QIN *, Shan CHEN, Jingyun ZHAO, Xu YANG (✉)

Hubei Key Laboratory of Genetic Regulation and Integrative Biology College of Life Science, Central China Normal University, Wuhan 430079, China

Abstract **To assess the biological safety of Fe_3O_4 nanoparticles (NPs), the oxidative-damage effect of these NPs was studied. Twenty-five Kunming mice were exposed to Fe_3O_4 NPs by intraperitoneal injection daily for 1 week at doses of 0, 10, 20, and 40 mg·kg^{-1}. Five Kunming mice were also injected with 40 mg·kg^{-1} ordinary Fe_3O_4 particles under the same physiological conditions. Biomarkers of reactive oxygen species (ROS), glutathione (GSH), and malondialdehyde (MDA) in the hepatic and brain tissues were detected. Results showed that no significant difference in oxidative damage existed at concentrations lower than 10 mg·kg^{-1} for NPs compared with the control group. Fe_3O_4 NP concentration had obvious dose–effect relationships ($P < 0.05$ or $P < 0.01$) with ROS level, GSH content, and MDA content in mouse hepatic and brain tissues at > 20 mg·kg^{-1} concentrations. To some extent, ordinary Fe_3O_4 particles with 40 mg·kg^{-1} concentration also affected hepatic and brain tissues in mice. The biological effect was similar to Fe_3O_4 NPs at 10 mg·kg^{-1} concentration. Thus, Fe_3O_4 NPs had significant damage effects on the antioxidant defense system in the hepatic and brain tissues of mice, whereas ordinary Fe_3O_4 had less influence than Fe_3O_4 NPs at the same concentration.**

Keywords Fe_3O_4 nanoparticle (NP), ordinary Fe_3O_4 particle, oxidative damage, reactive oxygen species (ROS), glutathione (GSH), malondialdehyde (MDA)

Introduction

Nanoparticles (NPs) are special materials with two or three dimensions ranging from 1 nm to 100 nm. Given the size, chemical composition, and shape of NPs, they have unusual physical and chemical characteristics (Fadeel and Garcia-Bennett, 2010) and are thus used in various fields. NPs can be used in drug delivery, gene delivery, cancer therapy, disease detection, biochemical sensing, bioimaging (Lippacher et al., 2001; Bystrzejewski et al., 2007; Nakamura et al., 2010; Pissuwan et al., 2011), and so on. When NPs are used for imaging or drug delivery, they can be coated with macromolecules such as DNA, proteins, or monoclonal antibodies to attach interested cells. In the progress of the interaction between NPs and cells, ensuring the safety of an organism is very important (Lewinski et al., 2008).

Adverse effects of NPs on organisms have been reported, including damage to aquatic microorganisms caused by boron NPs (Strigul et al., 2009), damage to human lung epithelial cells caused by ZnO and TiO_2 NPs (Hsiao and Huang, 2011), oxidative stress induced by NPs in human lung carcinoma cells (Valodkar et al., 2011), and so on. Four factors affect NP toxicity, i.e., chemical composition, small size, large surface-to-volume ratio, and surface property.

NPs are often classified as organic NPs such as fullerenes and inorganic NPs, which consist of metals (e.g., gold and silver) and metal oxides (e.g., iron oxide, titanium dioxide, silicon dioxide, etc.). Given the magnetic, mechanical, and optical properties of iron oxide NPs, they have extensive applications. On account of the magnetic properties of iron oxide NPs, they can be used to conduct tumor hyperthermia treatment (Xie et al., 2009). The magnetic properties of iron oxide NPs are also applied in the super paramagnetic iron

Received March 19, 2013; accepted August 7, 2013

Correspondence: Xu YANG

E-mail: yangxu@mail.ccnu.edu.cn

*These authors contributed equally to this work

oxide particle imaging instrument for magnetic resonance imaging that can be used to study cell tracking (Fleige et al., 2002). Iron oxide NPs can also be applied in drug and gene delivery. A doxorubicin-loaded system based on dextran cross-linked iron oxide NPs has been synthesized, and results show that the use of such NPs in drug delivery is possible (Yu et al., 2008). Fe_3O_4 NPs are a type of iron oxide NPs widely used in many fields, including printing ink manufacture, metal ion removal, magnetite filtration, biomolecule separation, and nuclear magnetic resonance imaging. The unique magnetic properties of Fe_3O_4 NPs have been largely exploited. Given the simplicity of their synthesis and partial solubility in acidic media compared with other nanoparticles like TiO_2 and SiO_2, Fe_3O_4 NPs have become a research hotspot (Ma et al., 2012). However, data on Fe_3O_4 NPs safety are lacking. Inconsistent results have increased confusion regarding this topic. Thus, the safety of Fe_3O_4 NPs must be studied.

Reactive oxygen species (ROS) can be classified into two different types, i.e., radical ROS (superoxide anion and hydroxyl radical) and non-radical ROS (hydrogen peroxide and hypochlorous acid). Considering the existence of active oxygen functional groups, ROS have very high activity in the body. Radicals emerge during the normal metabolic processes of humans. Some mechanisms can clear radicals, such as glutathione (GSH) that can be used to clear ROS. Under normal conditions, a balance exists between the generation and clearance of radicals that does not negatively affect the body (Xia et al., 2008). However, if the amount of ROS produced is too much that it cannot be handled by normal removal mechanisms such as GSH, ROS accumulation and can damage the structure of cells, thereby affecting their functions. The strong oxidability of ROS can oxidate biomembranes, and the end-product of lipid oxidation is malondialdehyde (MDA). Thus, ROS, GSH, and MDA are usually used as biomarkers of oxidative damage to measure the toxicity of a material.

Materials and methods

Reagents and apparatus

Fe_3O_4 NPs (Sigma, St Louis, MO, USA), ordinary Fe_3O_4 particles, 2′7′-dichlorodihydrofluorescein (DCFH-DA; Calbiochem, La Jolla, CA, USA), 5,5′-dithiobis-(2-nitrobenzoic acid) (DTNB; Sigma), and 2-thiobarbituric acid (TBA; Shanghai Reagent Factory, Shanghai, China) were used in experiments. All other chemicals used were analytical grade.

A low-temperature refrigerated centrifuge (Eppendorf-5417R), a continuous-wave and fluorescent microplate spectrophotometer (Bio-teck FLX800, USA), and a fluorescence spectrophotometer (Hitachi F-4500, Japan) were used in the experiment.

Experimental animals

Thirty SPF Kunming male mice (weight $\approx$ 24–28 g) were purchased from the Experimental Animal Center of Hubei Province (Wuhan, China). The mice were randomly grouped into 5 treatment groups with 6 mice per group. Three groups were exposed to an Fe_3O_4 nanoparticle environment (exposure doses = 10, 20, and 40 $mg \cdot kg^{-1}$). One experiment group was exposed to ordinary Fe_3O_4 particles at a dose of 40 $mg \cdot kg^{-1}$. The control group had PBS taking the place of oxide metal material. The experimented mice were housed in different cages at room temperature and fed with normal diet and water. Fe_3O_4 NPs was injected into mice through intraperitoneal injection. The volume of NPs injected to mice was based on their weights at a proportion of 1% $mL \cdot g^{-1}$. Mice were given daily intraperitoneal injections of NPs for 7 days continuously. The time of intraperitoneal injections was limited between 12:00 and 13:00 every day.

Preparation and characterization of Fe_3O_4 NPs

Fe_3O_4 NPs (diameter < 50 nm) were suspended in PBS (pH 7.5) to create solutions with concentration of 10, 20, and 40 $mg \cdot mL^{-1}$ as required. Normal Fe_3O_4 particles (microscale diameter) were suspended in PBS (pH 7.5) to obtain a solution with 40 $mg \cdot mL^{-1}$ concentration. A sonication time of 20 min was used only before each injection to make the solution homogeneous. The diameters of NPs and the crystal appearance were determined by scanning electron microscopy (SEM).

Sample preparation

The mice were sacrificed at noontime on the eighth day. Their brains and livers were quickly separated and rinsed with ice-cold PBS (0.01 $mol \cdot L^{-1}$, pH 7.5). All livers and brains were quickly dried, weighed and homogenized with 10 $mL \cdot g^{-1}$ ice-cold PBS (pH 7.5) using a homogenizer (about 0.3 g of tissue) on ice. The supernatants were then collected by centrifuging the homogenate at $10^4 \times g$ and 4 °C for 10 min, and this supernatant was used to measure ROS, GSH, and MDA.

ROS assay

About 100 μL of the supernatant diluted 40× with PBS (pH 7.5) was transferred to a 96-well microplate. Then, 100 μL of 5 $\mu mol \cdot L^{-1}$ DCFH-DA was immediately added to the microplate, which was slightly shaken and kept from light for 10 min. The fluorescence of dichlorofluoroscein (DCF), the oxidized product of DCFH-DA that can indicate the level of the ROS in a cell, was measured using a microplate spectrofluorometer with an excitation of 485 nm and emission of 525 nm (Elbekai and El-Kadi, 2005).

GSH assay

GSH is a thiol that is the major cleaner of ROS in organisms. GSH contains sulfhydryl that can react with DTNB to produce yellow compounds in the dark (Anderson, 1985). Measurement of the absorbance of yellow compounds (TNB) within the wavelength range of 405 and 414 nm can enable the accurate estimation of GSH in a sample, thereby avoiding disturbance from proteins with thiols. The supernatant was added to the organic solvent (1:3 butyl alcohol: trichloromethane) to precipitate the proteins. After mixing, centrifugation was performed at 10^4 rpm for 5 min. About 50 μL of the supernatant was transferred to a 96-well microplate, quickly added with 150 μL of 60 μg/mL DTNB solution, and kept in darkness for 5 min. The absorbance value of TNB was analyzed at a wavelength of 412 nm. Based on the standard curve, the GSH concentration was calculated.

MDA assay

At high temperatures (90–100 °C), the reaction of MDA and TBA results in an MDA-TBA adduct and can be measured colorimetrically at 530–540 nm under acidic conditions. Thus, 0.4 mL of tissue supernatant was mixed with 0.6% TBA solution (dissolved in 1 mol/L NaOH and added with 10% TCA) in a centrifugal tube. After a 15 min bath in boiling water, cooling on ice, and centrifuged at $10^4 \times g$ for 5 min, supernatants were collected for absorbance measurement at 450, 532, and 600 nm. The MDA concentration was calculated according to the formula C (μmol/L) = 6.45 ($A_{532} - A_{600}$) − 0.56A_{450}.

Statistical analysis

All data shown in this paper are expressed as the mean ± standard error of the mean and analyzed and plotted using Origin 6.0 software. Both one-way ANOVA and Tukey's test were applied to evaluate significant differences between groups. $p < 0.05$ was considered to be statistically significant, and $p < 0.01$ was considered to be very significant.

Results

After 7 days of continuous intraperitoneal injection of the different concentrations of Fe_3O_4 NPs and normal Fe_3O_4 particles in the mice for 1 week, the characteristics of Fe_3O_4 NPs, ROS levels, GSH content, MDA quantity, and DNA–protein cross-links coefficients of mouse hepatic and brain cells were determined. Results are shown in Figs. 1 to 6.

Characterization of Fe_3O_4 NPs

To characterize the appearance of Fe_3O_4 NPs used in the experiment, the crude particle appearance and dispersive diameter were detected. As shown in the SEM image in Figure 1, the particles were smoothly spherical. After ultrasonication dispersal, the distribution of particle diameters was observed, as shown in Fig. 2. A normal distribution curve with an axis of 35 nm was obtained, and NPs with diameters smaller than 50 nm were > 95%.

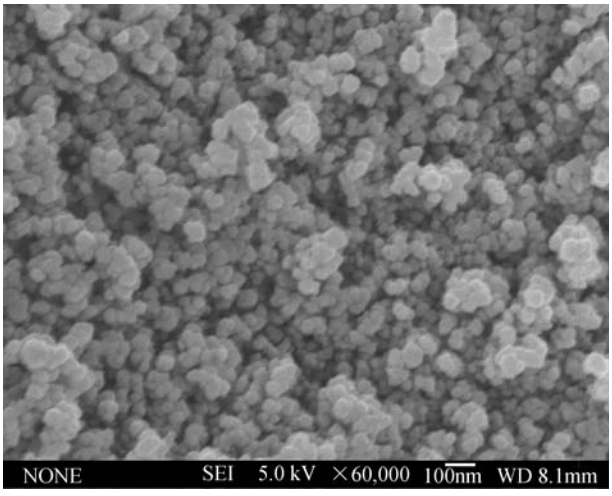

Figure 1 SEM image showing the crystal appearance of Fe_3O_4 NPs.

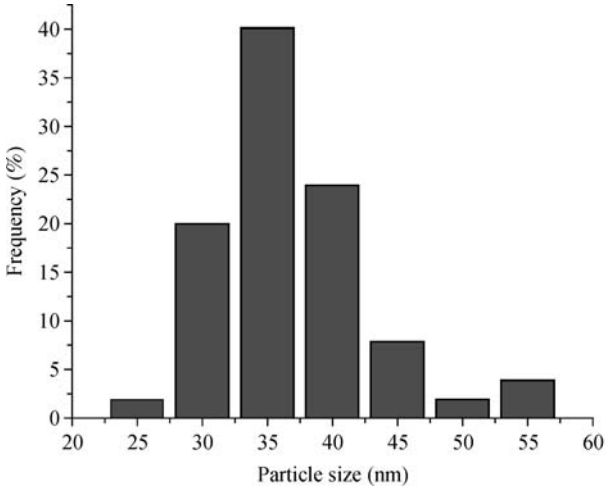

Figure 2 Size distribution of Fe_3O_4 NPs dispersed in phosphate-buffered saline.

Generation of ROS

Compared with the blank control, ROS generation both in brains and livers increased with increased Fe_3O_4 NP concentration, and the ROS level significantly increased at 20 mg·kg^{-1}·d^{-1} and 40 mg·kg^{-1}·d^{-1} Fe_3O_4 NPs ($p < 0.01$). Normal Fe_3O_4 particles at 40 mg·kg^{-1}·d^{-1} concentration only led to a significance change in the ROS level of hepatic cells ($p < 0.05$), whereas the ROS level of brain issue did not

significantly increase compared with the PBS control group. Fe_3O_4 NPs obviously affected the hepatic cells.

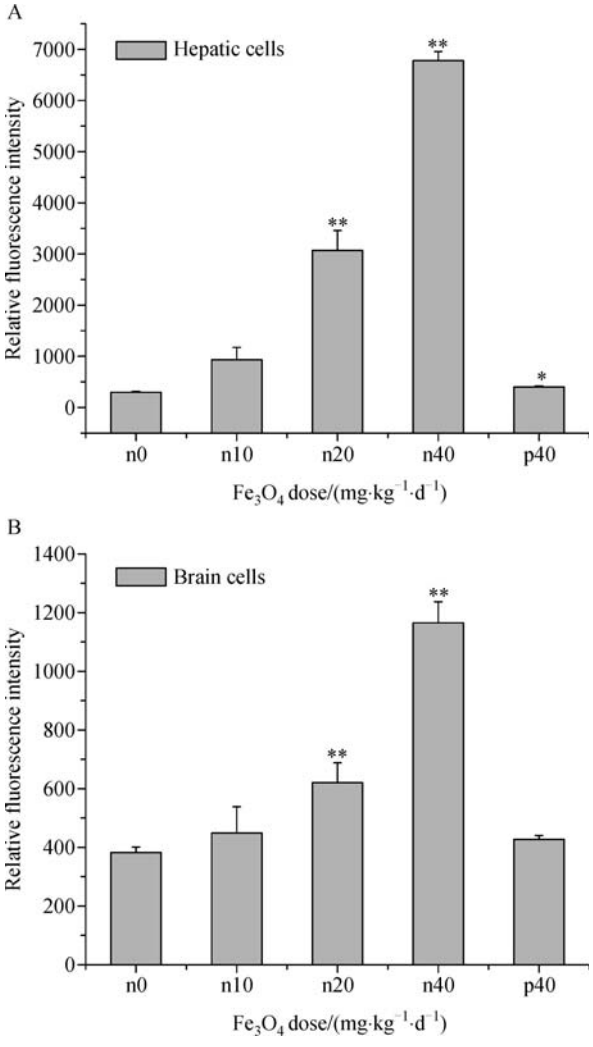

Figure 3 Effects of different concentration of NPs and normal Fe_3O_4 particles with a concentration of 40 $mg \cdot kg^{-1} \cdot d^{-1}$ (right-hand most) on the levels of ROS in mouse livers (A) and brains (B). $*p < 0.05$ and $**p < 0.01$, compared with the blank control group. Notes: n indicates NPs, and p indicates normal particles.

GSH content

The GSH content at different concentrations of Fe_3O_4 NPs and normal Fe_3O_4 particles are shown in Fig. 4. In livers, the decrease in GSH level was significant at 20 $mg \cdot kg^{-1} \cdot d^{-1}$ Fe_3O_4 NPs and 40 $mg \cdot kg^{-1} \cdot d^{-1}$ normal Fe_3O_4 particles ($p < 0.05$). The 40 $mg \cdot kg^{-1} \cdot d^{-1}$ Fe_3O_4 NP group was associated with a very significant decrease in GSH content ($p < 0.01$). The low-concentration Fe_3O_4 NP group did not show significant difference. The trends were similar in the brain, but the 20 $mg \cdot kg^{-1} \cdot d^{-1}$ Fe_3O_4 NPs showed a more significant decrease in GSH content ($p < 0.01$).

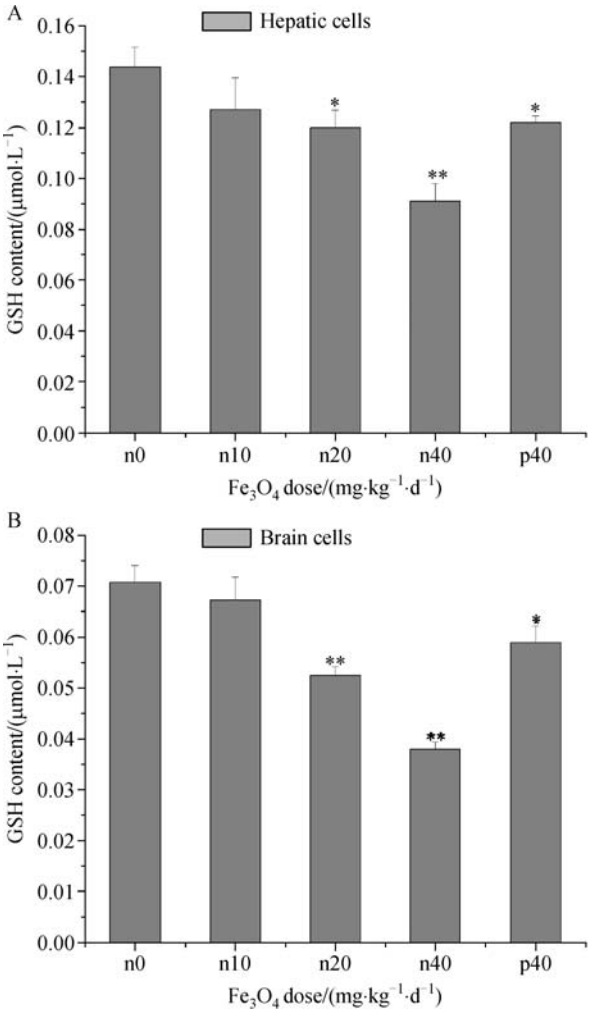

Figure 4 Effects of different concentration of NPs and normal Fe_3O_4 particles at a concentration of 40 $mg \cdot kg^{-1} \cdot d^{-1}$ (right-hand most) on the GSH content in mouse livers (A) and brains (B). $*p < 0.05$ and $**p < 0.01$, compared with the blank control group.

MDA concentration

Figure 5 demonstrates that the MDA content increased with increased concentration of Fe_3O_4 NPs in both livers and brains. When the concentration increased to 40 $mg \cdot kg^{-1} \cdot d^{-1}$, a very significant effect ($p < 0.01$) was observed both in livers and brain. Compared with the blank control group, only a slight effect was found upon exposure to normal Fe_3O_4 particles in both livers and brain. At the same concentration, MDA increased more in Fe_3O_4 NPs than in normal Fe_3O_4 particles.

Discussion

The chemical composition and morphology of a material crucially affect its chemical and physical properties. Mor-

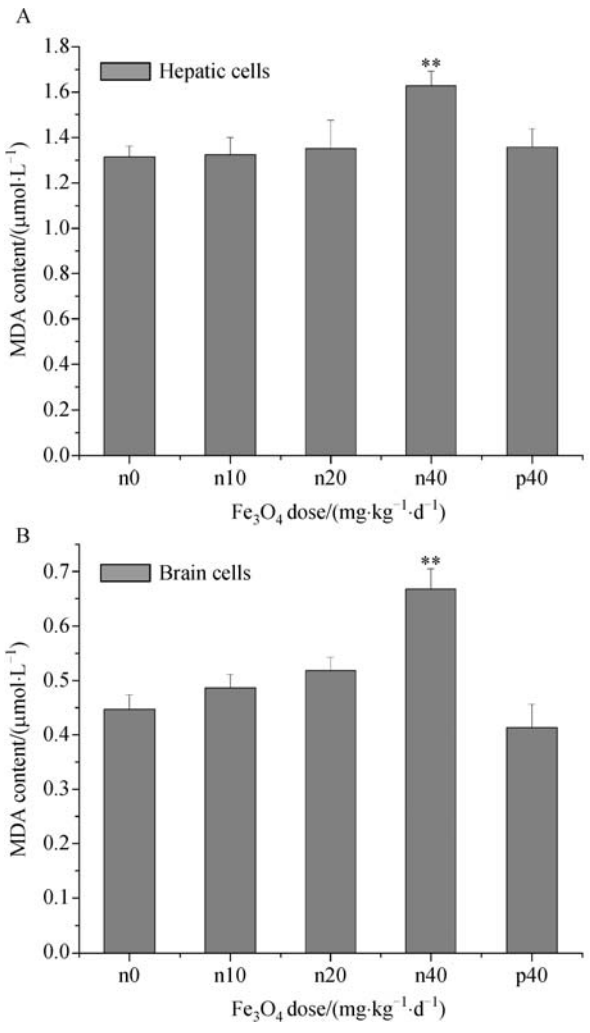

Figure 5 Effects of different concentration of NPs and normal Fe_3O_4 particles at a concentration of 40 $mg \cdot kg^{-1} \cdot d^{-1}$ (right-hand most) on the MDA concentration in mouse livers (A) and brains (B). *$p < 0.05$ and **$p < 0.01$, compared with the blank control group.

phology includes geometric shape, granularity, and particle distribution. In this study, the effects of normal Fe_3O_4 particles and Fe_3O_4 NPs on mouse liver and brain were compared in terms of their composition and particle size.

Particle size is a very important factor affecting NP cytotoxicity. No effect was detected at 100 $mg \cdot kg^{-1}$ with $\geqslant$300 nm nano-SiO_2, whereas liver damage already occurs at 30 $mg \cdot kg^{-1}$ with smaller-sized nano-SiO_2 (Nishimori et al., 2009). Single-walled carbon nanotubes are more toxic than multi-walled carbon nanotubes (Jia et al., 2005). A study on mice contaminated with different sizes of Fe_2O_3 particles shows that nano-Fe_2O_3 can markedly decrease pathological response (Zhu et al., 2008). In the present study, ordinary Fe_3O_4 had less influence than Fe_3O_4 NPs at the same concentration. Thus, the size of Fe_3O_4 particles is critical to the toxicity of such particles.

Many reports have shown that NPs can give rise to stress reaction and lead to oxidative damage (Kim et al., 2009; Tedesco et al., 2010; Piao et al., 2011; Novotna et al., 2012). In the current work, we determined the toxicity of a material by detecting oxidative damage in mouse liver and brain after exposure to NPs. Figure 3 shows that in contrast to the PBS control group, increased Fe_3O_4 NP concentration showed obviously increased ROS level. Moreover, the ROS level and NP concentration had an obvious dose–effect relationship and the increasing trend in the liver was more obvious. One explanation for the increase in ROS was that after the Fe_3O_4 NPs entered the body through intraperitoneal injection, the NPs were regarded as exogenous substances and induced some reactions in the body. Consequently, the balance in the body was broken, so the production of ROS exceeded the clearance ability of the body and ROS began to accumulate. NPs can pass organ barriers such as the blood–brain barrier (Borm and Kreyling, 2004), so Fe_3O_4 NPs can lead to more serious oxidative stress than normal Fe_3O_4 particles in the brain. Figure 3 shows that the ROS level at 20 $mg \cdot kg^{-1} \cdot d^{-1}$ Fe_3O_4 NPs obviously overtopped the ROS level at 40 $mg \cdot kg^{-1} \cdot d^{-1}$ normal Fe_3O_4 particles in the brain. The former can induce a very significant change ($p < 0.01$) compared with the PBS control group, but the latter only slightly changed compared with the PBS control group. Thus, Fe_3O_4 NPs can easily accumulate in the brain and induce more substantial damage than normal Fe_3O_4 particles. MDA content is a secondary indicator of oxidative damage; when ROS damages lipids, MDA increases. Similar to ROS, obvious dose–effect relationships ($p < 0.05$ or $p < 0.01$) were observed between Fe_3O_4 NP concentrations and MDA content. Figure 5 shows an obvious increase in MDA content at 40 $mg \cdot kg^{-1} \cdot d^{-1}$ Fe_3O_4 NPs in the brain. By contrast, normal Fe_3O_4 particles showed only slight changes in MDA content in the brain at the same concentration. The results can also lead to the same aforementioned conclusion, i.e., NPs accumulated to a degree that can pass the blood–brain barrier to inflict damage to the brain. The reduction in GSH showed that the proteins fighting oxidative stress decreased because of the lack of proteins that can clear ROS, and protein dysfunction may have occurred. Figure 4 shows that different from the effect on the liver, the particle size had greater effects on brain than liver. In the brain, 20 $mg \cdot kg^{-1} \cdot d^{-1}$ Fe_3O_4 NPs can induce a very significant change ($p < 0.01$), but 40 $mg \cdot kg^{-1} \cdot d^{-1}$ normal Fe_3O_4 particles showed a significant change ($p < 0.01$). These results demonstrated that the Fe_3O_4 NPs definitely induced more damage than normal Fe_3O_4 particles, especially in the brain. The low concentration of Fe_3O_4 NPs (20 $mg \cdot kg^{-1} \cdot d^{-1}$) can induce only limited ROS including superoxide anion, hydrogen peroxide, and hydroxyl radical. Correspondingly, GSH excited in the cytoplasm can clear the excess ROS.

Results showed that at 20 $mg \cdot kg^{-1} \cdot d^{-1}$ NPs, the ROS level in the liver showed a very significant difference from the PBS control group ($p < 0.01$). However, GSH in the liver only showed a significant difference ($p < 0.05$), and MDA in the

liver did not show an obvious difference from the PBS control group ($p > 0.05$). When foreign substances invade the body, the first reaction is the accumulation of ROS, so the change in ROS is the most obvious and the significant difference emerges first. Then, the accumulation of ROS can change the GSH and MDA contents, so ROS level is the most sensitive indicator of oxidative damage among the three. With increased concentration, the significance of GSH and MDA can be gradually observed. GSH comparison between liver and brain at 20 $mg \cdot kg^{-1} \cdot d^{-1}$ Fe_3O_4 NPs exceeded our expectation. The reason may be that the brain is more sensitive to changes in the internal environment than the liver. Thus, under the condition of low toxicity, the brain can produce a stronger signal.

Conclusions

The cytotoxicity of Fe_3O_4 on mouse hepatic and brain cells *in vivo* was studied. The following conclusions were drawn after analyzing the experimental results. First, results of ROS, GSH, and MDA demonstrated obvious dose–effect relationships ($p < 0.05$ or $p < 0.01$) between Fe_3O_4 NP concentrations and ROS level, GSH content, and MDA content in mouse hepatic and brain tissues. When the concentration was 10 $mg \cdot kg^{-1} \cdot d^{-1}$, Fe_3O_4 NPs also exerted some detectable effects. Second, among the three biomarkers, ROS was the most sensitive indicator and oxidative damage was first presented by ROS. Third and last, ordinary Fe_3O_4 had less influence than Fe_3O_4 NPs at the same concentration, so the particle size was very closely related to the toxicity of particles.

Acknowledgements

This work was financially supported by a grant from the National Natural Science Foundation of China (Grant No. 50802032).

Compliance with ethics guidelines

Yongli Wang, Nian Qin, Shan Chen, Jingyun Zhao and Xu Yang declare that they have no conflict of interest.

All institutional and national guidelines for the care and use of laboratory animals were followed.

References

Anderson M E (1985). Determination of glutathione and glutathione disulfide in biological samples. Methods Enzymol, 113: 548–555

Borm P J, Kreyling W (2004). Toxicological hazards of inhaled nanoparticles—potential implications for drug delivery. J Nanosci Nanotechnol, 4(5): 521–531

Bystrzejewski M, Cudziło S, Huczko A, Lange H, Soucy G, Cota-Sanchez G, Kaszuwara W (2007). Carbon encapsulated magnetic nanoparticles for biomedical applications: thermal stability studies. Biomol Eng, 24(5): 555–558

Elbekai R H, El-Kadi A O (2005). The role of oxidative stress in the modulation of aryl hydrocarbon receptor-regulated genes by As^{3+}, Cd^{2+}, and Cr^{6+}. Free Radic Biol Med, 39(11): 1499–1511

Fadeel B, Garcia-Bennett A E (2010). Better safe than sorry: Understanding the toxicological properties of inorganic nanoparticles manufactured for biomedical applications. Adv Drug Deliv Rev, 62 (3): 362–374

Fleige G, Seeberger F, Laux D, Kresse M, Taupitz M, Pilgrimm H, Zimmer C (2002). In vitro characterization of two different ultrasmall iron oxide particles for magnetic resonance cell tracking. Invest Radiol, 37(9): 482–488

Hsiao I L, Huang Y J (2011). Effects of various physicochemical characteristics on the toxicities of ZnO and TiO nanoparticles toward human lung epithelial cells. Sci Total Environ, 409(7): 1219–1228

Jia G, Wang H F, Yan L, Wang X, Pei R J, Yan T, Zhao Y L, Guo X B (2005). Cytotoxicity of carbon nanomaterials: single-wall nanotube, multi-wall nanotube, and fullerene. Environ Sci Technol, 39(5): 1378–1383

Kim S, Choi J E, Choi J, Chung K H, Park K, Yi J, Ryu D Y (2009). Oxidative stress-dependent toxicity of silver nanoparticles in human hepatoma cells. Toxicol In Vitro, 23(6): 1076–1084

Lewinski N, Colvin V, Drezek R (2008). Cytotoxicity of nanoparticles. Small, 4(1): 26–49

Lippacher A, Müller R H, Mäder K (2001). Preparation of semisolid drug carriers for topical application based on solid lipid nanoparticles. Int J Pharm, 214(1-2): 9–12

Ma P, Luo Q, Chen J, Gan Y, Du J, Ding S, Xi Z, Yang X (2012). Intraperitoneal injection of magnetic Fe_3O_4-nanoparticle induces hepatic and renal tissue injury via oxidative stress in mice. Int J Nanomedicine, 7: 4809–4818

Nakamura M, Ozaki S, Abe M, Doi H, Matsumoto T, Ishimura K (2010). Size-controlled synthesis, surface functionalization, and biological applications of thiol-organosilica particles. Colloids Surf B Biointerfaces, 79(1): 19–26

Nishimori H, Kondoh M, Isoda K, Tsunoda S, Tsutsumi Y, Yagi K (2009). Silica nanoparticles as hepatotoxicants. Eur J Pharm Biopharm, 72(3): 496–501

Novotna B, Jendelova P, Kapcalova M, Rossner P Jr, Turnovcova K, Bagryantseva Y, Babic M, Horak D, Sykova E (2012). Oxidative damage to biological macromolecules in human bone marrow mesenchymal stromal cells labeled with various types of iron oxide nanoparticles. Toxicol Lett, 210(1): 53–63

Piao M J, Kang K A, Lee I K, Kim H S, Kim S, Choi J Y, Choi J, Hyun J W (2011). Silver nanoparticles induce oxidative cell damage in human liver cells through inhibition of reduced glutathione and induction of mitochondria-involved apoptosis. Toxicol Lett, 201(1): 92–100

Pissuwan D, Niidome T, Cortie M B (2011). The forthcoming applications of gold nanoparticles in drug and gene delivery systems. J Control Release, 149(1): 65–71

Strigul N, Vaccari L, Galdun C, Wazne M, Liu X, Christodoulatos C, Jasinkiewicz K (2009). Acute toxicity of boron, titanium dioxide, and aluminum nanoparticles to Daphnia magna and Vibrio fischeri. Desalination, 248(1–3): 771–782

Tedesco S, Doyle H, Blasco J, Redmond G, Sheehan D (2010). Oxidative stress and toxicity of gold nanoparticles in Mytilus edulis. Aquat Toxicol, 100(2): 178–186

Valodkar M, Jadeja R N, Thounaojam M C, Devkar R V, Thakore S (2011). In vitro toxicity study of plant latex capped silver nanoparticles in human lung carcinoma cells. Mater Sci Eng C, 31 (8): 1723–1728

Xia T, Kovochich M, Liong M, Mädler L, Gilbert B, Shi H, Yeh J I, Zink J I, Nel A E (2008). Comparison of the mechanism of toxicity of zinc oxide and cerium oxide nanoparticles based on dissolution and oxidative stress properties. ACS Nano, 2(10): 2121–2134

Xie J, Huang J, Li X, Sun S, Chen X (2009). Iron oxide nanoparticle platform for biomedical applications. Curr Med Chem, 16(10): 1278–1294

Yu M K, Jeong Y Y, Park J, Park S, Kim J W, Min J J, Kim K, Jon S (2008). Drug-loaded superparamagnetic iron oxide nanoparticles for combined cancer imaging and therapy in vivo. Angew Chem Int Ed Engl, 47(29): 5362–5365

Zhu M T, Feng W Y, Wang B, Wang T C, Gu Y Q, Wang M, Wang Y, Ouyang H, Zhao Y L, Chai Z F (2008). Comparative study of pulmonary responses to nano- and submicron-sized ferric oxide in rats. Toxicology, 247(2-3): 102–111